A porous media transport model for apple drying

C. Kumar[a,d], M. U. H. Joardder[b], T.W. Farrell[c], G.J. Millar[d] and M. A. Karim[a]

[a] School of Chemistry, Physics and Mechanical Engineering, Queensland University of Technology, Brisbane, Australia
[b] Department of Mechanical Engineering, RUET, Rajshahi, Bangladesh.
[c] School of Mathematical Sciences, Queensland University of Technology, Brisbane, Australia
[d] Institute for Future Environments, Queensland University of Technology, Brisbane, Australia
[e] Salisbury Research Facility, Department of Agriculture and Fisheries, Queensland Government, Brisbane, Australia

ABSTRACT

A comprehensive multiphase porous media model was developed and validated for apple drying. Thermal, transport, and structural properties of apple required to develop such model were formulated and presented. The model considered the transport of liquid water by capillary diffusion and gas pressure, and the transport of vapour by binary diffusion and gas pressure. A non-equilibrium formulation was used to calculate the evaporation rate, which enabled the separate illustration of vapour and liquid water transport. The equations were solved by finite element method (FEM) using physics-based modelling and a simulation platform (COMSOL Multiphysics). The model predictions were validated using experimental data and good agreement was found. Spatial distribution of liquid water and vapour saturation curves showed that the saturation levels were lower on and near the surface compared to the centre of the food material. The convective and diffusive fluxes of liquid water and vapour were presented, and this data suggested that the fluxes were higher on and near the surface of the sample.

Keywords: modelling; food drying; porous media; apple; COMSOL Multiphysics

Nomenclature

Abbreviations

MPMM	Multiphase porous media models
CV-FE	Control volume finite element modelling

Symbols

c_w	Mass concentrations of water (kg m^{-3})
c_v	Mass concentrations of vapour (kg m^{-3})
c_a	Mass concentrations of air (kg m^{-3})
$c_{p\,eff}$	Effective specific heat (J kg^{-1} K^{-1})
c_{pw}	Specific heat capacity of water (J kg^{-1} K^{-1})
c_{pg}	Specific heat capacity of gas (J kg^{-1} K^{-1})
c_{ps}	Specific heat capacity of solid (J kg^{-1} K^{-1})
D_c	Capillary diffusivity (m^2 s^{-1})
D_T	Thermal diffusivity (m^2 s^{-1})
$D_{eff,g}$	Effective binary diffusivity of vapour and air (m^2 s^{-1})
D_{va}	Binary diffusivity of vapour and air (m^2 s^{-1})
H	Sample thickness (m)
h_g	Enthalpy of gas (J)
h_w	Enthalpy of water (J)
h_{fg}	Latent heat of evaporation (J kg^{-1})
h_{mv}	Mass transfer coefficient (m s^{-1})
h_T	Heat transfer coefficient (W m^{-2} K^{-1})
K_{evap}	Evaporation constant
k_w	Intrinsic permeability of water (m^2)
$k_{r,w}$	Relative permeability of water (m^2)
k_g	Intrinsic permeability of gas (m^2)

60	$k_{r,g}$	Relative permeability of gas (m^2)
61	k_{eff}	Effective thermal conductivity (W m^{-1} K^{-1})
62	$k_{th,g}$	Thermal conductivity of gas (W m^{-1} K^{-1})
63	$k_{th,w}$	Thermal conductivity of water (W m^{-1} K^{-1})
64	$k_{th,s}$	Thermal conductivity of solid (W m^{-1} K^{-1})
65	M_{db}	Moisture content dry basis
66	M_{wb}	Moisture content wet basis
67	M_g	Molecular weight of gas (kg mol^{-1})
68	M_v	Molecular weight of vapour (kg mol^{-1})
69	$\vec{n}_w$	Water mass flux (kg m^{-2} s^{-1})
70	$\vec{n}_v$	Vapour mass flux (kg m^{-2} s^{-1})
71	$\vec{n}_g$	Gas mass flux (kg m^{-2} s^{-1})
72	$\vec{n}_{v,total}$	Total vapour flux at the surface (kg m^{-2} s^{-1})
73	P	Total gas pressure (Pa)
74	P_0	Incident microwave power (W)
75	p_v	Partial pressure of vapour (Pa)
76	p_a	Partial pressure of air (Pa)
77	p_c	Capillary pressure (Pa)
78	$p_{v,eq}$	Equilibrium vapour pressure (Pa)
79	$P_{v,sat}$	Saturation vapour pressure (Pa)
80	$p_{v,air}$	Vapour pressure of ambient air (Pa)
81	P_{amb}	Ambient pressure (Pa)
82	R	Universal gas constant (J mol^{-1} K^{-1})
83	R_{evap}	Evaporation rate of liquid water to water vapour (kg m^{-3} s^{-1})
84	S_w	Saturation of water
85	S_g	Saturation of gas
86	S_{w0}	Initial water saturation

87	S_{v0}	Initial saturation of vapour
88	S_{g0}	Initial gas saturation
89	T	Temperature of product (^{0}C)
90	T_{air}	Drying air temperature (^{0}C)
91	V	Drying air velocity (m s^{-1})
92	Z	Distance from vertical axis from origin (m)
93	ΔV	Representative elementary volume (m^3)
94	ΔV_g	Volume of gas (m^3)
95	ΔV_w	Volume of water (m^3)
96	ΔV_s	Volume of solid (m^3)
97	t_{eq}	Equilibration time (s)
98	φ	Apparent porosity
99	φ_0	Initial equivalent porosity,
100	μ_w	Viscosity of water (Pa s)
101	μ_g	Viscosity of gas (Pa s)
102	ω_v	Mass fraction of vapour
103	ω_a	Mass fraction of air
104	ρ_s	Solid density (kg m^{-3})
105	ρ_w	Density of water (kg m^{-3})
106	ρ_g	Density of gas (kg m^{-3})
107	ρ_g	Density of gas phase (kg m^{-3})
108	ρ_{eff}	Effective density (kg m-^{3})

109

110 1. INTRODUCTION

111 Modelling of food drying is a complex problem due to issues such as the intricate
112 physical structure of the materials of interest. Many modelling efforts have been reported in
113 the literature for transport in food materials such as drying (Barati and Esfahani, 2011,
114 Diamante et al., 2010, Kumar et al., 2012, Kumar et al., 2016b, Karim and Hawlader, 2005a,

115 Karim and Hawlader, 2005b, Kumar et al., 2015), frying (Ni and Datta, 1999), microwave
116 heating (Ni et al., 1999, Rakesh et al., 2010), thawing (Chamchong and Datta, 1999a), baking
117 (Zhang et al., 2005), and puffing (Rakesh and Datta, 2013) etc. These models can be classified
118 into two broad categories; empirical and theoretical models (Kumar et al., 2014). Empirical or
119 observation-based models can be developed rapidly and are quite effective. However, they do
120 not provide a physical insight into the process and exhibit limited predictive capability. By
121 contrast, physics-based models are preferred as predictive models not only in food drying but
122 also in areas outside of the food industry. Among these theoretical approaches, diffusion based
123 models are very popular because of their simplicity and as such have been used by many
124 researchers (Chandra Mohan and Talukdar, 2010, Perussello et al., 2012, Kumar et al., 2016b,
125 Perussello et al., 2014). Diffusion models assume conductive heat transfer for energy and
126 diffusive transport for moisture. These models need diffusivity values which have to be
127 experimentally determined. Although these models can provide a good match with
128 experimental results, they cannot provide a detailed understanding of other transport
129 mechanisms such as pressure driven flow. Lumping all the water transport processes as
130 diffusion cannot be justified under all situations. The drawbacks of these kind of models has
131 been discussed in detail in the work of Zhang and Datta (2004).

132 The next group of models with improved formulation compared to diffusion models are
133 those that assume a sharp moving boundary between dry and wet regions. This type of model
134 has been applied to deep fat frying (Farkas et al., 1996) and is characterised as an analogue to
135 the freezing and thawing models used for a pure substance (Mascarenhas et al., 1997).
136 Recently, distributed evaporation models, in contrast to sharp boundary models, have become
137 popular. Datta (2007a) termed these distributed evaporation models as mechanistic models
138 because these models considered heat and mass transfer equations for each phase (solid, liquid,
139 gas plus vapour) in porous media. They are termed multiphase porous media models (MPMM).
140 These MPMM models rigorously study the transition from the individual phase at the
141 'microscopic' level to the representative average volume at the 'macroscopic' level (Whitaker,
142 1977). Furthermore, they are computationally effective and consequently have been applied
143 to a wide range of food processing applications such as frying (Ni and Datta, 1999, Bansal et
144 al., 2014), microwave heating (Rakesh et al., 2010, Chen et al., 2014), puffing (Rakesh and
145 Datta, 2013) baking (Zhang et al., 2005), meat cooking (Dhall and Datta, 2011) etc. However,
146 application of these models to drying processes has been limited.

147 Some multiphase models have been applied to: (a) vacuum drying (Turner and Perré,
148 2004); (b) convection drying (Stanish et al., 1986) of wood and clay (Chemkhi et al., 2009);
149 (c) microwave spouted bed drying of apples (Feng et al., 2001); and (d) large bagasse stockpiles
150 (Farrell et al., 2012). A common issue that is integral to MPMM is the assumption that the
151 vapour and water phases are in equilibrium. Equilibrium conditions may not be valid for lower
152 moisture content of the sample during drying; thus, equilibrium conditions may never be
153 achieved at the surface since transport rates are relatively high there. Therefore, a non-
154 equilibrium approach appears to be a more realistic representation of the physical situation
155 during drying (Zhang and Datta, 2004). Using equilibrium vapour pressure in a drying model
156 is likely to overestimate the drying rate because equilibrium may not be achieved
157 instantaneously at the surface due to low moisture content. The non-equilibrium approach for
158 evaporation can be used to express evaporation, thus allowing the calculation of each phase
159 separately. The equations resulting from non-equilibrium models provide a better description
160 of the physics involved and facilitate calculation of evaporation behaviour. Recently, Zhang
161 *et al*. (2012) applied a multiphase model to a non-equilibrium formulation for evaporation.
162 Nevertheless, they only used the model for vacuum drying of corn and the simulation results
163 were not compared with any experimental data (Zhang and Kong, 2012). There are some
164 MPMM models available for other processing systems (but not for drying) such as frying (Ni
165 and Datta, 1999, Bansal et al., 2014), microwave heating (Rakesh et al., 2010, Chen et al.,
166 2014), puffing (Rakesh and Datta, 2013) and baking (Zhang et al., 2005). However, all these
167 formulations were only for potato, a single product. Beyond this volume averaging approach,
168 Carr et al. (2013a) developed a dual scale model to simulate the drying behaviour of
169 hygroscopic porous media. The model coupled the porous medium with the pore structure in
170 the microscale. Carr *et al.* (2013b, 2011) also developed an innovative mesoscopic model
171 based on control volume finite element modelling (CV-FE) and a variable step-size Jacobian-
172 free exponential integrator for simulating transport in heterogeneous porous media. Notably,
173 these models were applied to drying of wood. The non-equilibrium multiphase porous media
174 model for drying of apple can provide fundamental understanding of transport process of
175 different phases and optimization of the drying process. Therefore, the aim of this work was to
176 present the necessary dynamic properties to develop an MPMM for apple. The specific
177 objectives of this study were to:

178 • formulate real-time materials properties for MPMM of apple drying

- develop a multiphase porous media model using non-equilibrium formulations for transport of liquid water, vapour, and energy during drying of apple
- investigate heat and mass transport during drying

2. MATHEMATICAL MODEL

The model equations for multiphase porous media were developed describing heat, mass, and momentum transfer within an apple slice (food material) during convection drying. The equations also represent the transport mechanism, assumptions and input parameters for the model.

The model developed in this research considered transport of liquid water, vapour, and air inside food materials. The mass and energy conservation equations included convection, diffusion, and evaporation. Momentum conservation was developed from Darcy's equations. Evaporation was considered as being distributed throughout the domain, and a non-equilibrium evaporation formulation was used for evaporation-condensation phenomena.

2.1 PROBLEM DESCRIPTION AND ASSUMPTIONS

A schematic diagram of the domain and the simplifications used to formulate the governing equations for general three-dimensional porous media are presented in Fig. 1. A two-dimensional axisymmetric geometry of a three-dimensional apple slice was considered for simulation. Heat and mass transfer took place at all boundaries except the symmetry boundary. The apple slice was considered as a porous medium and the pores were filled with three transportable phases, namely liquid water, air and water vapour as shown in Fig. 1.

Fig. 1. Can be inserted near here

All phases (solid, liquid, and gases) were continuous and local thermal equilibrium was valid, which meant that the temperatures in all three phases were equal. Liquid water transport occurred due to convective flow resulting from gas pressure gradient, capillary flow and evaporation. Vapour and air transport arose from gas pressure gradients and binary diffusion.

2.2 GOVERNING EQUATIONS

The mathematical model consisted of the conservation equations for all the transportable phases and transport mechanisms discussed above.

207 **2.2.1 Mass balance equations**

208 The representative elementary volume ΔV (m^3) was the sum of the volume of three
209 phases, namely, gas, water, and solid,

$$\Delta V = \Delta V_g + \Delta V_w + \Delta V_s . \quad (1)$$

210 where, ΔV_g is the volume of gas (m^3), ΔV_w is the volume of water (m^3), and ΔV_s is the volume
211 of solid (m^3).

212 The apparent porosity, φ, was defined as the volume fraction occupied by gas and water.
213 Thus,

$$\varphi = \frac{\Delta V_g + \Delta V_w}{\Delta V} . \quad (2)$$

214 The water saturation, S_w, and gas saturation, S_g, were defined as the fraction of pore
215 volume occupied by that particular phase, namely,

$$S_w = \frac{\Delta V_w}{\Delta V_w + \Delta V_g} = \frac{\Delta V_w}{\varphi \Delta V} , \quad (3)$$

216 and

$$S_g = \frac{\Delta V_g}{\Delta V_w + \Delta V_g} = \frac{\Delta V_g}{\varphi \Delta V} = 1 - S_w , \quad (4)$$

217 respectively.

218 The mass concentrations of water, c_w (kg m^{-3}), vapour, c_v (kg m^{-3}),and air, c_a (kg m^{-3}),
219 were given by,

$$c_w = \rho_w \varphi S_w , \quad (5)$$

$$c_v = \frac{p_v M_v}{RT} \varphi S_g , \quad (6)$$

220 and

$$c_a = \frac{p_a M_a}{RT} \varphi S_g , \quad (7)$$

221 respectively.

Here, ρ_w is the density of water (kg m^{-3}), R is the universal gas constant (J mol^{-1} K^{-1}), and T is the temperature of product (K), p_v is the partial pressure of vapour (Pa), p_a is the partial pressure of air (Pa), M_a and M_v were molar mass of air and vapour, respectively (kg mol^{-1}).

The mass conservation equation for the liquid water was expressed by,

$$\frac{\partial}{\partial t}\left(\varphi S_w \rho_w\right) + \nabla \cdot \left(\vec{n}_w\right) = -R_{evap}, \tag{8}$$

where, $\vec{n}_w$ is water flux (kg m^{-2} s^{-1}), and R_{evap} is the evaporation rate of liquid water to water vapour (kg m^{-3} s^{-1}).

The total flux of the liquid water was due to the gradient of liquid pressure, $p_w = P - p_c$, as given Darcy's law (Bear, 1972), namely,

$$\vec{n}_w = -\rho_w \frac{k_w k_{r,w}}{\mu_w} \nabla p_w = -\rho_w \frac{k_w k_{r,w}}{\mu_w} \nabla P + \rho_w \frac{k_w k_{r,w}}{\mu_w} \nabla p_c . \tag{9}$$

Here, P is the total gas pressure (Pa), p_c is the capillary pressure (Pa), k_w is the intrinsic permeability of water (m^2), $k_{r,w}$ is the relative permeability of water, and μ_w is the dynamic viscosity of water (Pa s). More details on these parameters are discussed in section 2.6.

It should be noted that, the first term of Eq. (9) represents the flow due to gradients in gas pressure, which is significant only in the case of intensive heating such as microwave heating, deep fat frying, and contact heating at high temperature (Farkas et al., 1996, Ni and Datta, 1999, Bansal et al., 2014). The second term represents the flow due to capillary pressure.

The capillary pressure depends on concentration (c_w) and temperature (T) for a particular material (Datta, 2007a). Therefore, Eq. (9) can be rewritten as,

$$\vec{n}_w = -\rho_w \frac{k_w k_{r,w}}{\mu_w} \nabla P + \rho_w \frac{k_w k_{r,w}}{\mu_w} \frac{\partial p_c}{\partial c_w} \nabla c_w + \rho_w \frac{k_w k_{r,w}}{\mu_w} \frac{\partial p_c}{\partial T} \nabla T . \tag{10}$$

In turn, the second and third terms of Eq. (10) can be rewritten in terms of capillary diffusivity, D_c (m^2 s^{-1}), and thermal diffusivity, D_T (m^2 s^{-1}), given by,

$$D_c = -\rho_w \frac{k_w k_{r,w}}{\mu_w} \frac{\partial p_c}{\partial c_w}, \tag{11}$$

and

$$D_T = -\rho_w \frac{k_w k_{r,w}}{\mu_w} \frac{\partial p_c}{\partial T}, \tag{12}$$

respectively.

The capillary diffusivity due to the temperature gradient, ∇T (K), is known as the Soret effect and is often less significant than the diffusivity due to concentration gradients (Datta, 2007a), and will thus be neglected in this work.

Substituting the above into Eq. (8) the concentration of liquid water can be written as,

$$\frac{\partial}{\partial t}\left(\varphi S_w \rho_w\right) + \nabla.\left(- \rho_w \frac{k_w k_{r,w}}{\mu_w} \nabla P - D_c \nabla c_w \right) = -R_{evap} \tag{13}$$

The conservation of water vapour can be written in terms of the mass fraction, ω_v, as

$$\frac{\partial}{\partial t}\left(\varphi S_g \rho_g \omega_v\right) + \nabla.\left(\vec{n}_v\right) = R_{evap}, \tag{14}$$

where, ρ_g is the density of gas (kg m^{-3}), ω_v is the mass fraction of vapour and $\vec{n}_v$ is the vapour mass flux (kg m^{-2} s^{-1}).

For a binary mixture $\vec{n}_v$ can be written as (Bird et al., 2007),

$$\vec{n}_v = -\rho_g \omega_v \frac{k_g k_{r,g}}{\mu_v} \nabla P - \varphi S_g \rho_g D_{eff,g} \nabla \omega_v, \tag{15}$$

where, k_g is the intrinsic permeability of gas (m^2), $k_{r,g}$ is the relative permeability of gas (m^2), μ_g is the viscosity of gas (Pa s) and $D_{eff,g}$ is the binary diffusivity of vapour and air (m^2 s^{-1}).

The gas phase is a mixture of vapour and air. After calculating the mass fraction of vapour, ω_v, from Eq. (15), the mass fraction of air, ω_a, can be calculated from

$$\omega_a = 1 - \omega_v. \tag{16}$$

2.2.2 Continuity equation to solve for pressure

The gas phase is assumed to consist of an ideal mixture of water vapour and air. The gas pressure, P, may be determined via a total mass balance for the gas phase, namely,

$$\frac{\partial}{\partial t}\left(\rho_g \varphi S_g\right) + \nabla.\left(\vec{n}_g\right) = R_{evap}\,, \tag{17}$$

where, the gas flux, $\vec{n}_g$, is given by,

$$\vec{n}_g = -\rho_g \frac{k_g k_{r,g}}{\mu_i} \nabla P\,. \tag{18}$$

Here ρ_g is the density of gas phase, given by,

$$\rho_g = \frac{PM_g}{RT}, \tag{19}$$

where, M_g is the molar mass of gas (kg mol^{-1}).

2.2.3 Energy equation

It was assumed that each of the phases were in thermal equilibrium and thus the energy balance equation was written as,

$$\rho_{eff} c_{p\,eff} \frac{\partial T}{\partial t} + \nabla.\left(\vec{n}_g h_g + \vec{n}_w h_w\right) = \nabla.(k_{eff} \nabla T) - h_{fg} R_{evap}\,. \tag{20}$$

Here, T is the temperature (K) of each phase, h_g is the enthalpy of gas (J), h_w is the enthalpy of water (J), h_{fg} is the latent heat of evaporation (J kg^{-1}), ρ_{eff} is the effective density (kg m^{-3}), $c_{p\,eff}$ is the effective specific heat capacity (J kg^{-1} K^{-1}), and k_{eff} is the effective thermal conductivity (W m^{-1} K^{-1}). Equation (20) considered energy transport due to conduction and convection, and energy sources/sinks due to evaporation/condensation.

The effective thermal conductivity and density of the materials were calculated by the volume-weighted average of the different phases as given by Eq. (21) and (22), respectively (Kumar et al., 2016a, Chen et al., 2014, Dhall and Datta, 2011).

$$k_{eff} = \varphi\left(S_g k_{th,g} + S_w k_{th,w}\right) + (1-\varphi) k_{th,s} \tag{21}$$

and

$$\rho_{eff} = \varphi\left(S_g \rho_g + S_w \rho_w\right) + (1-\varphi)\rho_s\,. \tag{22}$$

The effective specific heat capacity of the materials was obtained from the mass fraction's arithmetic average of the material,

$$c_{p_{eff}} = m_g\left(\omega_g c_{pg} + \omega_a c_{pa}\right) + m_w c_{pw} + m_s c_{ps}\,. \tag{23}$$

Here ρ_s is the solid density (kg m^{-3}); c_{pg}, c_{pw}, and c_{ps} are the specific heat capacity of gas, water, and solid (J kg^{-1} K^{-1}), respectively; $k_{th,g}$, $k_{th,w}$, and $k_{th,s}$ are the thermal conductivity of gas, water, and solid, (W m^{-1} K^{-1}) and m_g, m_w and m_s are the mass fraction of gas, water and solid, respectively.

2.3 EVAPORATION RATE

A non-equilibrium formulation as described in Ni *et al.* (1999) was considered to calculate the evaporation rate inside the sample, namely,

$$R_{evap} = K_{evap}\frac{M_v}{RT}\left(p_{v,eq} - p_v\right) \text{ for } 0 \le r < r_s \; and \; 0 \le z < z_s \tag{24}$$

Here, M_v is the molar mass of vapour (kg mol^{-1}), $p_{v,eq}$ is the equilibrium vapour pressure (Pa), p_v is the vapour pressure (Pa), and K_{evap} is the evaporation constant (s^{-1}) that is material and process-dependent and given by the reciprocal of equilibration time, t_{eq}, (discussed later in this section). The surface evaporation rate was taken into account *via* the boundary condition given by Eq. (35).

The equilibrium vapour pressure can be obtained from the sorption isotherm for different materials. Ratti *et al.* (1989) developed a correlation for sorption isotherms from different materials at a particular temperature and moisture content at any point of the sample. The equilibrium vapour pressure, $p_{v,eq}$, for apple is given by,

$$p_{v,eq} = P_{v,sat}(T)exp\left(-0.182M_{db}^{\;-0.696} + 0.232e^{-43.949M}M_{db}^{\;0.0411}\ln[P_{sat}(T)]\right). \tag{25}$$

Here, $P_{v,sat}$ is the saturated vapour pressure of water (Pa) and M_{db} is the moisture content (dry basis), which can be related to S_w via,

$$M_{db} = \frac{\varphi S_w \rho_w}{(1-\varphi)\rho_s}\,. \tag{26}$$

The saturated vapour pressure of water, $P_{v,sat}$, is a function of temperature and is given by Vega-Mercado *et al.* (2001) as,

$$P_{v,sat} = \exp\begin{bmatrix} -5800.2206/T + 1.3915 - 0.0486T + 0.4176\times10^{-4}T^2 \\ -0.01445\times10^{-7}T^3 + 6.656\ln(T) \end{bmatrix}. \quad (27)$$

295 The vapour pressure, p_v, is obtained from partial pressure relations given by,

$$p_v = \chi_v P, \quad (28)$$

296 where, χ_v is the mole fraction of vapour and P is the total pressure (Pa).

297 The mole fraction of vapour, χ_v, can be calculated from the mass fractions and molar
298 mass of vapour and air as,

$$\chi_v = \frac{\omega_v M_a}{\omega_v M_a + \omega_a M_v}, \quad (29)$$

299 where, M_a is the molar mass of air (kg mol^{-1}) and M_v is the molar mass of vapour (kg mol^{-1}).

300 As noted above, K_{evap}, was given by the reciprocal of the equilibration time t_{eq}. The
301 value of t_{eq} depended upon the ratio of the gas phase volume in the pores in which vapour has
302 to diffuse, and the surface area available for evaporation (Halder et al., 2010). This ratio scaled
303 as the radius of the pore (in the case of simple cylindrical pores). The time taken for a water
304 molecule to make the transition from liquid water to water vapour was $10^{-14}\,s$ (1999, Halder et
305 al., 2010). Using this condition and assuming pure diffusion of vapour from the evaporating
306 surface, the time to equilibrium at one mean free path 1 μm away from the liquid surface was
307 less than $10^{-6}\,s$, and that of 25 μm away was around $10^{-5}\,s$ (Ward and Fang, 1999). The time
308 scale analysis presented by Halder *et al.* (2010) showed that all the transport time scales were
309 greater than the equilibration time scale for food materials with a maximum pore size smaller
310 than 25 μm (*e.g.* potato, meat, etc.). Experiments showed that the pore size (mean pore
311 diameter) of the apple sample studied was approximately 50 μm (Joardder et al., 2014).
312 Therefore, the equilibration time, t_{eq}, was considered as 10^{-3} s and thus the value of the
313 evaporation constant to be 10^3 s^{-1}.

314 **2.4 INITIAL CONDITIONS**

315 The initial conditions for Eqs. (13), (15), (17), and (20) were given by,

$$c_{w(t=0)} = \rho_w \varphi S_{w0}, \quad (30)$$

$$w_{v(t=0)} = 0.0262\,, \tag{31}$$

$$P_{(t=0)} = P_{amb}\,, \tag{32}$$

316 and

$$T_{(t=0)} = 303K\,, \tag{33}$$

317 respectively. Here, ρ_w is the density of water (kg m^{-3}) and S_{w0} is the initial saturation of water.

318 **2.5 BOUNDARY CONDITIONS**

319 The total vapour flux, $\vec{n}_{v,total}$, from a hypothetical surface with only gas phase can be
320 written as,

$$\vec{n}_{v,total} = h_{mv}\frac{\left(p_v\text{-}p_{v\,air}\right)}{RT}, \tag{34}$$

321 where, $\vec{n}_{v,total}$ is the total vapour flux at the surface (kg m^{-2} s^{-1}), $p_{v,air}$ is the vapour pressure of
322 ambient air (Pa) and h_{mv} is the mass transfer coefficient (m s^{-1}).

323 However, in a multiphase problem, the vapour flux on the surface will be a contribution
324 from evaporation from liquid water, and water vapour already present at the surface. Therefore,
325 assuming the volume fraction is equal to the surface area fraction, the boundary conditions for
326 water and vapour phase can be written as,

$$\vec{n}_w = h_{mv}\varphi S_w\frac{\left(p_v\text{-}p_{v\,air}\right)}{RT}, \tag{35}$$

$$\vec{n}_v = h_{mv}\varphi S_g\frac{\left(p_v\text{-}p_{v\,air}\right)}{RT}, \tag{36}$$

327 respectively.

328 In most of the food processes, the pressure at the boundary (exposed to environment) is
329 equal to the ambient pressure, P_{amb}. Hence, the boundary condition for continuity Eq. (17)
330 was expressed as,

$$P = P_{amb}\,. \tag{37}$$

For the energy equation (Eq. (20)), the energy can transferred by convective heat transfer and heat can be lost due to evaporation at the surface, given by,

$$q_{surf} = h_T (T - T_{air}) + h_{mv} \varphi S_w \frac{(p_v - p_{v\,air})}{RT} h_{fg} . \quad (38)$$

Here, h_T is the heat transfer coefficient (W m^{-2} K^{-1}) and T_{air} is the drying air temperature (K). In the symmetry boundaries, no flux boundary conditions were used for all transport equations.

2.6 INPUT PARAMETERS

The input parameters of the model are listed in Table 1. The parameters that are not listed in Table 1, were derived and discussed in the following sub-sections.

Table 1 can be inserted near here

2.6.1 Permeability

Permeability is an important factor in order to describe the water transport due to pressure gradient in unsaturated porous media. The value of the permeability determines the extent of pressure generation inside the material. The smaller the permeability, the lower the moisture transport and the higher the internal pressure, and vice versa.

The permeability of a material, k, is a product of intrinsic permeability, k_i, and relative permeability, $k_{i,r}$, (Bear, 1972), namely,

$$k = k_i k_{i,r} . \quad (39)$$

Measurement of permeability values for deformable hygroscopic materials such as food is difficult (Ni, 1997). The intrinsic permeability depends on pore structure of the materials and several models have been used to calculate intrinsic permeability (Feng et al., 2004). The intrinsic permeability for apple tissue can be obtained by the Kozeny-Carman model, given by,

$$k_w = 5.578 \times 10^{-12} \frac{\varphi_g^{\,3}}{(1 - \varphi_g)^2} \qquad (0.39 < \varphi_g < 0.77) \quad . \quad (40)$$

The gas intrinsic permeability k_g was $7.4 \times 10^{-12} \pm 1.2 \times 10^{-12}$ m^2 and $6.5 \times 10^{-13} \pm 2.4 \times 10^{-13}$ m^2 at moisture levels of 36.0% (db) and 60.0% (db) respectively. In

this study, an average of 4.0×10^{-12} m^2 (Feng et al., 2004) computational reduce to used was time processing and costs. However, the relative permeabilities were considered as moisture dependent.

Relative permeabilities are generally expressed as functions of liquid saturation. There are numerous studies which have developed such functions (Plumb, 1991). In this study, the relative permeability of water, $k_{r,w}$, and gas, $k_{r,g}$, for apple were obtained from the measurements by Feng *et al.* (2004), namely,

$$k_{r,w} = S_w^{\ 3}, \tag{41}$$

and

$$k_{r,g} = 1.01e^{-10.86S_w}, \tag{42}$$

respectively.

The relative permeabilities using the above equations were plotted in Fig. 2 for better illustration.

Fig. 2 can be inserted near here

2.6.2 Viscosity of water and gas

Viscosities of water (Truscott, 2004) and gas (Gulati and Datta, 2013) as a function of temperature are given by,

$$\mu_w = \rho_w e^{\left(-19.143+\frac{1540}{T}\right)} \tag{43}$$

and

$$\mu_g = 0.017\times10^{-3}\left(\frac{T}{273}\right)^{0.65}. \tag{44}$$

Here T is the temperature of the product (K).

2.6.3 Effective gas diffusivity

The effective gas diffusivity can be calculated as a function of gas saturation and porosity according to the Bruggeman correction (Ni, 1997) given by,

$$D_{eff,g} = D_{va}\left(S_g \varphi\right)^{4/3}. \tag{45}$$

373 Here, binary diffusivity, D_{va}, can be written as,

$$D_{va} = 2.3\times10^{-5}\frac{P_0}{P}\left(\frac{T}{T_0}\right)^{1.81}, \tag{46}$$

374 where $T_0 = 256$ K and $P_0 = 1$ atm. For simplicity, in this study effective gas diffusivity was
375 considered as 2.6×10^{-5} m^2 s^{-1} (Datta, 2007).

376 **2.6.4 Capillary diffusivity of liquid water**

377 Capillary diffusivity of liquid water is important for both convection and microwave
378 drying. Capillary force is the main driving force of liquid water in convective drying if there
379 is no pressure gradient developed (Ni, 1997). Although there is a large amount data concerning
380 the effective moisture diffusivity data for apples available in the literature, these were obtained
381 by fitting diffusion models to experimental drying curves and are not equal to capillary
382 diffusivity.

383 It is clear in our formulation that the capillary diffusivity, D_c, is proportional to $\frac{\partial p_c}{\partial S_w}$,
384 and is a function of capillary pressure given by Eq. (11). The typical relationship between
385 capillary pressure and water saturation is shown in Fig. 3 (Bear, 1972).

386 **Fig. 3 can be inserted near here**

387 It can be seen that the capillary pressure increases significantly at lower saturation levels
388 and when it reaches irreducible saturation the value becomes infinity. Therefore, that part is
389 neglected to avoid numerical instability. From Fig. 3 we can see that near $S_w = 1$, $\frac{\partial p_c}{\partial S_w}$ is
390 almost infinity, therefore D_c became very large. The underlying physics was that as S_w
391 approached 1, more water became free, and the resistance of the solid matrix to the flow of free
392 water was almost zero. Therefore, D_c was very large at high moisture content; as a result, the
393 concentration gradient was concomitantly small (Ni, 1997). As an outcome, the capillary
394 diffusivity can be very close to effective moisture diffusivity for very wet material when vapour
395 diffusion is insignificant. However, it can be quite different in the lower moisture region. Ni

(1997) used Eq. (47) for capillary diffusivity of potato for low to high moisture content where it was assumed that the capillary diffusivity was only moisture dependent:

$$D_c = 10^{-8} \exp(-2.8 + 2M_{db}). \quad (47)$$

A similar function was developed here for apple by analysing the value of different effective diffusivity values presented in the literature (Golestani et al., 2013, Esturk, 2012, Feng et al., 2000, Feng et al., 2001). Considering that the highest value corresponded to the highest saturation of water, a similar relationship between capillary diffusivity and moisture as given by Ni (1997) was used in this study, namely,

$$D_c = 10^{-8} \exp(-6.88 + 8M_{wb}). \quad (48)$$

2.6.5 Partial pressure of vapour in ambient condition

The partial pressure of vapour in an ambient condition was a product of relative humidity (RH) and saturation vapour pressure $P_{v,sat}$ given by, $p_{v,air} = RH \times p_{sat}$. For RH = 70% and 30^0C, the specific humidity (moisture ratio) was 0.0188 kg [water] kg^{-1} [dry air]. During drying, the temperature was elevated to 60^0C at a specific humidity of 0.0188 0.0188 kg [water] kg^{-1} [dry air], where the relative humidity became only 15%. Therefore, the partial vapour pressure for drying air, $p_{v,air} = 0.15 \times 19947 = 2992$ Pa.

2.6.6 Heat and mass transfer coefficient

The heat and mass transfer coefficients were calculated based on the empirical relationship discussed in a previous paper (Kumar et al., 2016b) and found to be h_T =16.746 W m^{-2} K^{-1} and h_m =0.017904 m s^{-1}, respectively.

3. EXPERIMENTAL METHOD

Fresh Granny Smith apples obtained from local supermarkets were used for the convection drying experiments. The samples were stored at 5±1 ^{0}C to keep them as fresh as possible before they were used in the experiments. The apples taken from the storage were washed and put aside for one hour to allow its temperature to elevate to room temperature before each drying experiment. The samples were then sliced 10 mm thick with diameters of about 40 mm. Then the samples were put into a household convection dryer, and the temperature was set to 60 ^{0}C. Following each drying test, the sample was heated to 100 ^{0}C for

422 at least 24 h to get bone dry mass to calculate the initial moisture content of the apple slices
423 which was approximately 0.868 (w.b.). The moisture losses were recorded at regular intervals
424 of 10 min with a digital balance (specifications: model BB3000; Mettler-Toledo AG,
425 Grefensee, Switzerland 0.001g accuracy). The experiments were completed three times and
426 the standard deviation was calculated.

427 ## 4. NUMERICAL SOLUTION AND SIMULATION METHODOLOGY

428 The model was solved by using COMSOL Multiphysics 4.4a (COMOSOL Inc.
429 Stockholm, Sweden) a finite element analysis and simulation software. COMSOL is an
430 advanced engineering simulation software used for modelling and simulating any physical
431 process described by partial differential equations. The mesh used consisted of 3,376 elements
432 and a non-uniform mesh with grid refinement at the transport boundary (maximum element
433 size 0.1mm) was chosen as shown in Fig. 4.

434 **Fig. 4 can be inserted near here**

435 To ensure that the results were grid-independent, several grid sensitivity tests were
436 conducted. The time stepping period was chosen as one second (1s) to solve the equations.
437 The simulation was performed using Windows 7 with Intel Core i7 CPU, 3.4 GHz processor
438 and 24 GB of RAM and it took about 10 min to run the model.

439 ## 5. RESULTS AND DISCUSSION

440 In this section, profiles of moisture, temperature, pressure, fluxes and evaporation rate
441 are presented and discussed. Validation was also conducted by comparing moisture content
442 from experiments.

443 ### 5.1 Moisture content

444 The profile of average moisture content obtained from the model and experiments are
445 compared in Fig. 5. It can be seen that the model provided a satisfactory result with a R^2 value
446 of 0.997. The drying curve presented here had similar characteristics to those found in the
447 literature for apple drying (Yan Bai et al., 2002, Golestani et al., 2013). It was found that that
448 moisture content (dry basis) of apple slice dropped from its initial value of 6.6 to 2.9 kg [water]
449 kg^{-1} [dry air] after 150 min of drying.

450 **Fig. 5 can be inserted near here**

451 **5.2 Distribution and evolution of water and vapour**

452 The distribution of water saturation and vapour saturation along the half thickness of the
453 material at different times is shown in Fig. 6 and Fig. 7, respectively.

454 **Fig. 6 can be inserted near here**

455 As expected, the graphs showed that during drying the water and vapour saturation near
456 the surface was lower than in the central region. The water saturation decreased with drying
457 time at each point within the sample. Similar moisture distributions were found by Chemkhi
458 *et al.* (2009), particularly that the surface contained lower moisture content compared to the
459 core region.

460 **Fig. 7 can be inserted near here**

461 Unlike the moisture distribution, vapour saturation was found to increase with drying
462 time within the sample (as shown in Fig. 7). However, vapour saturation at and near the surface
463 was lower than in the centre, because the vapour coming into contact with the surface was
464 immediately convected away by the drying air.

465 **5.3 Temperature profile**

466 The temperature profile at the surface and centre of the material are shown in Fig. 8. The
467 surface temperature rose sharply at the beginning of the drying process (approximately 0 – 15
468 min); this was due to the sudden exposure of the material to a higher temperature. Chemkhi *et*
469 *al.* (2009) described this phase, where the material was heated until wet bulb temperature value
470 was reached, as the transient period. The temperature then rose at a slower rate until it reached
471 the drying air temperature. A similar profile of temperature at the surface during convection
472 drying of porous media was found by Chemki *et al.* (2009). They observed that it took about
473 330 min to raise the temperature to maximum (drying air temperature).

474 **Fig. 8 can be inserted near here**

475 The surface temperature was always higher than the centre temperature throughout the
476 drying period. The difference between the surface and centre temperature increased as drying
477 progressed. The reason behind this was presumably related to a decrease in the thermal
478 conductivity with moisture content.

5.4 Vapour pressures

Fig. *9* represents the comparison between vapour pressure, equilibrium vapour pressure and saturation vapour pressure at just below (0.1 mm underneath) the surface. These three vapour pressures were very important in relation to drying kinetics. The saturation vapour pressure varied with temperature given by Eq. (25) and data was available from many sources (Çengel and Boles, 2006). The saturation vapour pressure data available in (Çengel and Boles, 2006) was compared with simulated saturation data and found to be consistent. The equilibrium vapour pressure data was calculated from the sorption isotherm of apple given by Eq. (24) and, as expected, was found to be lower than the saturation vapour pressure. At the beginning of the drying process, vapour pressure at 0.1 mm beneath the surface was equal to equilibrium vapour pressure which meant the equilibrium condition was valid. However, when the moisture was removed from that point after approximately 10 min of drying, the vapour pressure became lower than the equilibrium vapour pressure causing non-equilibrium evaporation (according to Eq. 24) at that point which can be seen in Fig. 10. After that, when the moisture was removed from the point of interest after about 80 min of drying, equilibrium vapour pressure decreased and became equal with the vapour pressure. Thus, evaporation ceased; this occurred because after 80 min of drying the water saturation became almost zero *i.e.* no liquid water was available for evaporation.

Fig. 9 can be inserted near here

5.5 Evaporation rate

One of the advantages of non-equilibrium approaches over other methods in the modelling of drying is the ability to calculate evaporation. Fig. *10* shows that a higher evaporation rate occurred near the surface. In addition to this behaviour, the evaporation rate was higher in a narrow zone near the surface and nearly zero in other areas. It showed a significant amount of evaporation occurred at the beginning of the drying process (0 - 30 min). Halder *et al.* (2007) also found similar phenomena in frying, where production of excess amounts of vapour at the beginning caused vapour to move towards the centre.

According to Eq. (24), it can be said that difference between vapour pressure and equilibrium vapour pressure determines the evaporation rate. Therefore, evaporation was higher near the surface due to the large difference between the vapour pressure and equilibrium vapour pressure. A similar trend was found by Dhall *et al.* during meat cooking (2012).

Fig. 10 can be inserted here

Another interesting pattern emerged from the graph in Fig. 10, wherein evaporation started inside the material, and the rate decreased as drying progressed. It showed that the evaporation was very high at 30 min (amounting to 1.1 kg m^{-3} s^{-1}) and as drying progressed the maximum evaporation moved towards the centre. The reason behind this behaviour could be that the liquid water saturation became lower (drier) near the surface as drying progressed, and the difference between vapour pressure and equilibrium vapour pressure essentially became zero as discussed previously. Another possible explanation could be that the gradual penetration of heat increased the kinetic energy of water molecules which moved towards the centre. Thus, the peak evaporation gradually moved towards the centre. In addition to this observation, the decreasing evaporation rate found near the surface could be due to the relatively fewer water molecules available due to the lower moisture content.

5.6 Vapour and water fluxes

The major advantage of a multiphase porous media model is that the relative contribution of vapour and water fluxes due to diffusion and gas pressure gradient can be understood and illustrated. Moisture fluxes due to capillary pressure and gas pressure gradients are plotted in Fig. 11 and Fig. 12, respectively. It can be seen that the capillary flux was higher at about 0.5 – 1.0 mm beneath the surface and this peak moved towards the core. The explanation for this could be that the capillary flux ($D_c \nabla c_w$) was proportional to moisture gradient (∇c_w). The gradient was higher initially near that region and the peak of the gradient moved towards the core with time. At and near the surface, the water flux decreased, which could be due to the decrease in capillary diffusivity due to lower moisture content.

Fig. 11 can be inserted near here

The water flux due to the gas pressure gradient (Fig. 12) showed a similar pattern of flux distribution, albeit with a lower magnitude. The convective water flux increased from zero (at the centre) to a peak at approximately 1 mm beneath the surface. This could be due to the higher pressure gradient near the surface resulting in higher convective flow. However, in convection drying, the gradient of pressure required a closer inspection, because there may not be enough pressure development inside the sample. Although the pressure gradient was higher at and near the surface (0 – 1 mm beneath the surface), the flux due to gas pressure started to reduce in these regions. This could be due to the reduction of relative permeability of water

541 which tended to zero at lower moisture saturation, resulting in a convective term
542 $\left(-\rho_w \frac{k_w k_{r,w}}{\mu_w} \nabla P \right)$ near zero.

543 **Fig. 12 can be inserted near here**

544 Fig. *13* and Fig. *14* show the spatial distribution of the diffusive and convective fluxes of
545 vapour, respectively. The figures show that vapour fluxes from both sources mainly occurred
546 near the surface with zero in the core region. Ousegui *et al.* (2010) found a similar pattern of
547 vapour flux due to diffusion. This was due to the transport at the surface, which generated
548 large vapour concentration and pressure gradients near the surface which promoted higher
549 diffusion and convective flux, respectively.

550 **Fig. 13 and Fig. 14 can be inserted near here**

551 Generally, the vapour and water fluxes caused by all sources showed that the fluxes were
552 minimal at the centre and gradually increased towards the surface. Therefore, the centre
553 contained higher moisture saturation, even though the surface is already dried.

554 ## 6. CONCLUSIONS

555 A non-equilibrium multiphase porous media model, which was a significant
556 advancement relative to existing approaches, was developed for convection apple drying. The
557 necessary formulation of instantaneous properties for implementing the MPMM was presented
558 in detail. The model was validated by comparing experimental moisture and it was
559 demonstrated that good agreement existed. The results of this study supported the idea that the
560 surface dried first, and then the moisture from inside moved due to both capillary and gas
561 pressure. The model in this paper was used to elucidate the relative contribution of various
562 modes of transport and phase change, which cannot be investigated with a single phase model.
563 For example, parameters such as capillary diffusion, gas pressure and evaporation in overall
564 moisture transport were evaluated, which is not possible through experiments or by using
565 simpler models. The fundamental basis of the model enabled a deeper understanding of drying
566 kinetics and, thus, it can be an important tool in making safety, quality and product design
567 related predictions.

ACKNOWLEDGMENTS

The first author acknowledges the financial support from International Postgraduate Research Award (IPRS), Australian Postgraduate Award (APA) and Advance Queensland project to carry out this research. The authors are also grateful to Dr Steve Parkin for his careful edit.

7. REFERENCES

BANSAL, H. S., TAKHAR, P. S. & MANEEROTE, J. 2014. Modeling multiscale transport mechanisms, phase changes and thermomechanics during frying. *Food Research International,* 62**,** 709-717.

BARATI, E. & ESFAHANI, J. A. 2011. Mathematical modeling of convective drying: Lumped temperature and spatially distributed moisture in slab. *Energy,* 36**,** 2294-2301.

BEAR, J. 1972. *Dynamics of fluids in porous media*, American Elsevier Pub. Co.

BIRD, R. B., STEWART, E. W. & LIGHTFOOT, N. E. 2007. *Transport Phenomena*, John Wiley & Sons.

CARR, E., TURNER, I. & PERRÉ, P. 2013a. A Dual-Scale Modeling Approach for Drying Hygroscopic Porous Media. *Multiscale Modeling & Simulation,* 11**,** 362-384.

CARR, E. J., TURNER, I. W. & PERRÉ, P. 2011. A New Control-Volume Finite-Element Scheme for Heterogeneous Porous Media: Application to the Drying of Softwood. *Chemical Engineering & Technology,* 34**,** 1143-1150.

CARR, E. J., TURNER, I. W. & PERRÉ, P. 2013b. A variable-stepsize Jacobian-free exponential integrator for simulating transport in heterogeneous porous media: Application to wood drying. *Journal of Computational Physics,* 233**,** 66-82.

ÇENGEL, Y. A. & BOLES, M. A. 2006. *Thermodynamics: an engineering approach*, McGraw-Hill Higher Education.

CHAMCHONG, M. & DATTA, A. K. 1999a. Thawing of foods in a microwave oven: II. Effect of load geometry and dielectric properties. *Journal of Microwave Power and Electromagnetic Energy,* 34**,** 22-32.

CHANDRA MOHAN, V. P. & TALUKDAR, P. 2010. Three dimensional numerical modeling of simultaneous heat and moisture transfer in a moist object subjected to convective drying. *International Journal of Heat and Mass Transfer,* 53**,** 4638-4650.

CHEMKHI, S., JOMAA, W. & ZAGROUBA, F. 2009. Application of a Coupled Thermo-Hydro-Mechanical Model to Simulate the Drying of Nonsaturated Porous Media. *Drying Technology,* 27**,** 842-850.

CHEN, J., PITCHAI, K., BIRLA, S., NEGAHBAN, M., JONES, D. & SUBBIAH, J. 2014. Heat and Mass Transport during Microwave Heating of Mashed Potato in Domestic Oven—Model Development, Validation, and Sensitivity Analysis. *Journal of Food Science,* 79**,** E1991-E2004.

CHOI, Y. & OKOS, M. 1986. *Thermal properties of liquid foods: review,* MI, American soceity of agricultural engineers.

DATTA, A. K. 2007. Porous media approaches to studying simultaneous heat and mass transfer in food processes. II: Property data and representative results. *Journal of Food Engineering,* 80**,** 96-110.

610 DATTA, A. K. 2007a. Porous media approaches to studying simultaneous heat and mass
611 transfer in food processes. I: Problem formulations. *Journal of Food Engineering,* 80,
612 80-95.
613 DHALL, A. & DATTA, A. K. 2011. Transport in deformable food materials: A poromechanics
614 approach. *Chemical Engineering Science,* 66, 6482-6497.
615 DHALL, A., HALDER, A. & DATTA, A. K. 2012. Multiphase and multicomponent transport with
616 phase change during meat cooking. *Journal of Food Engineering,* 113, 299-309.
617 DIAMANTE, L. M., IHNS, R., SAVAGE, G. P. & VANHANEN, L. 2010. Short communication: A
618 new mathematical model for thin layer drying of fruits. *International Journal of Food*
619 *Science & Technology,* 45, 1956-1962.
620 ESTURK, O. 2012. Intermittent and Continuous Microwave-Convective Air-Drying
621 Characteristics of Sage (Salvia officinalis) Leaves. *Food and Bioprocess Technology,* 5,
622 1664-1673.
623 FARKAS, B. E., SINGH, R. P. & RUMSEY, T. R. 1996. Modeling heat and mass transfer in
624 immersion frying. I, model development. *Journal of Food Engineering,* 29, 211-226.
625 FARRELL, T. W., KNIGHT, J. H., MORONEY, T. J., HOBSON, P. A., TURNER, I. W. & FULFORD, G.
626 R. 2012. The mathematical modelling of large-scale bagasse stockpiles.
627 FENG, H., TANG, J., CAVALIERI, R. P. & PLUMB, O. A. 2001. Heat and mass transport in
628 microwave drying of porous materials in a spouted bed. *AIChE Journal,* 47, 1499-
629 1512.
630 FENG, H., TANG, J. & JOHN DIXON-WARREN, S. 2000. Determination of Moisture Diffusivity
631 of Red Delicious Apple Tissues by Thermogravimetric Analysis. *Drying Technology,*
632 18, 1183-1199.
633 FENG, H., TANG, J., PLUMB, O. A. & CAVALIERI, R. P. 2004. Intrinsic and relative permeability
634 for flow of humid air in unsaturated apple tissues. *Journal of Food Engineering,* 62,
635 185-192.
636 GOLESTANI, R., RAISI, A. & AROUJALIAN, A. 2013. Mathematical modeling on air drying of
637 apples considering shrinkage and variable diffusion coefficient *Drying Technology,*
638 31, 40-51.
639 GULATI, T. & DATTA, A. K. 2013. Enabling computer-aided food process engineering:
640 Property estimation equations for transport phenomena-based models. *Journal of*
641 *Food Engineering,* 116, 483-504.
642 HALDER, A., DHALL, A. & DATTA, A. K. 2007. An Improved, Easily Implementable, Porous
643 Media Based Model for Deep-Fat Frying: Part II: Results, Validation and Sensitivity
644 Analysis. *Food and Bioproducts Processing,* 85, 220-230.
645 HALDER, A., DHALL, A. & DATTA, A. K. 2010. Modeling Transport in Porous Media With Phase
646 Change: Applications to Food Processing. *Journal of heat transfer,* 133, 031010-
647 031010.
648 JOARDDER, M. U. H., KUMAR, C. & KARIM, A. 2014. Food Microstructure: The bridging factor
649 between process parameter and food quality. *Critical Reviews in Food Science and*
650 *Nutrition,* In press.
651 KARIM, M. A. & HAWLADER, M. N. A. 2005a. Mathematical modelling and experimental
652 investigation of tropical fruits drying. *International Journal of Heat and Mass*
653 *Transfer,* 48, 4914-4925.
654 KARIM, M. A. & HAWLADER, M. N. A. 2005b. Drying characteristics of banana: theoretical
655 modelling and experimental validation. *Journal of Food Engineering,* 70, 35-45.

656 KUMAR, C., JOARDDER, M. U. H., FARRELL, T. W. & KARIM, A. 2016a. Multiphase porous
657 media model for intermittent microwave convective drying (IMCD) of food.
658 *International Journal of Thermal Science* 104**,** 304-314.
659 KUMAR, C., JOARDDER, M. U. H., FARRELL, T. W., MILLAR, G. J. & KARIM, M. A. 2015. A
660 Mathematical Model for Intermittent Microwave Convective (IMCD) Drying of Food
661 Materials. *Drying Technology,* 34**,** 962-973.
662 KUMAR, C., KARIM, A., JOARDDER, M. U. H. & MILLER, G. Modeling heat and mass transfer
663 process during convection drying of fruit. The 4th International Conference on
664 Computational Methods 2012 Gold Coast, Australia.
665 KUMAR, C., KARIM, M. A. & JOARDDER, M. U. H. 2014. Intermittent drying of food products:
666 A critical review. *Journal of Food Engineering,* 121**,** 48-57.
667 KUMAR, C., MILLAR, G. J. & KARIM, M. A. 2016b. Effective Diffusivity and Evaporative Cooling
668 in Convective Drying of Food Material. *Drying Technology,* 33**,** 227-237.
669 MASCARENHAS, W. J., AKAY, H. U. & PIKAL, M. J. 1997. A computational model for finite
670 element analysis of the freeze-drying process. *Computer Methods in Applied*
671 *Mechanics and Engineering,* 148**,** 105-124.
672 NI, H. 1997. *Multiphase moisture transport in porous media under intensive microwave*
673 *heating.* PhD, Cornell University, Ithaca, New York, United States.
674 NI, H. & DATTA, A. K. 1999. Moisture, Oil and Energy Transport During Deep-Fat Frying of
675 Food Materials. *Food and Bioproducts Processing,* 77**,** 194-204.
676 NI, H., DATTA, A. K. & TORRANCE, K. E. 1999. Moisture transport in intensive microwave
677 heating of biomaterials: a multiphase porous media model. *International Journal of*
678 *Heat and Mass Transfer,* 42**,** 1501-1512.
679 OUSEGUI, A., MORESOLI, C., DOSTIE, M. & MARCOS, B. 2010. Porous multiphase approach for
680 baking process – Explicit formulation of evaporation rate. *Journal of Food*
681 *Engineering,* 100**,** 535-544.
682 PERUSSELLO, C. A., KUMAR, C., DE CASTILHOS, F. & KARIM, M. A. 2014. Heat and mass
683 transfer modeling of the osmo-convective drying of yacon roots (Smallanthus
684 sonchifolius). *Applied Thermal Engineering,* 63**,** 23-32.
685 PERUSSELLO, C. A., MARIANI, V. C. & DO AMARANTE, Á. C. C. 2012. Numerical and
686 experimental analysis of the heat and mass transfer during okara drying. *Applied*
687 *Thermal Engineering*.
688 PLUMB, O. A. 1991. Heat Transfer During Unsaturated Flow in Porous Media. *In:* KAKAÇ, S.,
689 KILKIŞ, B., KULACKI, F. & ARINÇ, F. (eds.) *Convective Heat and Mass Transfer in*
690 *Porous Media.* Springer Netherlands.
691 RAHMAN, M. S. 2008. *Food properties handbook*, CRC press.
692 RAKESH, V. & DATTA, A. K. 2013. Transport in deformable hygroscopic porous media during
693 microwave puffing. *AIChE Journal,* 59**,** 33-45.
694 RAKESH, V., DATTA, A. K., WALTON, J. H., MCCARTHY, K. L. & MCCARTHY, M. J. 2012.
695 Microwave combination heating: Coupled electromagnetics- multiphase porous
696 media modeling and MRI experimentation. *AIChE Journal,* 58**,** 1262-1278.
697 RAKESH, V., SEO, Y., DATTA, A. K., MCCARTHY, K. L. & MCCARTHY, M. J. 2010. Heat transfer
698 during microwave combination heating: Computational modeling and MRI
699 experiments. *AIChE Journal,* 56**,** 2468-2478.
700 RATTI, C., CRAPISTE, G. H. & ROTSTEIN, E. 1989. A New Water Sorption Equilibrium
701 Expression for Solid Foods based on Thermodynamic Considerations. *Journal of Food*
702 *Science,* 54**,** 738-742.

STANISH, M. A., SCHAJER, G. S. & KAYIHAN, F. 1986. A mathematical model of drying for hygroscopic porous media. *AIChE Journal,* 32**,** 1301-1311.
TRUSCOTT, S. 2004. *A heterogenous three-dimensional computational model for wood drying*. PhD, Queensland University of Technology.
TURNER, I. W. & PERRÉ, P. 2004. Vacuum drying of wood with radiative heating: II. Comparison between theory and experiment. *AIChE Journal,* 50**,** 108-118.
VEGA-MERCADO, H., MARCELA GÓNGORA-NIETO, M. & BARBOSA-CÁNOVAS, G. V. 2001. Advances in dehydration of foods. *Journal of Food Engineering,* 49**,** 271-289.
WARD, C. A. & FANG, G. 1999. Expression for predicting liquid evaporation flux: Statistical rate theory approach. *Physical Review E,* 59**,** 429-440.
WHITAKER, S. 1977. Simultaneous Heat, Mass, and Momentum Transfer in Porous Media: A Theory of Drying. *In:* JAMES, P. H. & THOMAS, F. I. (eds.) *Advances in Heat Transfer.* Elsevier.
YAN BAI, RAHMAN, M. S., PERERA, C. O., SMITH, B. & MELTON, L. D. 2002. Structural Changes in Apple Rings during Convection Air-Drying with Controlled Temperature and Humidity. *J Agric Food Chem,* 50**,** 3179-3185.
ZHANG, J. & DATTA, A. K. 2004. Some Considerations in Modeling of Moisture Transport in Heating of Hygroscopic Materials. *Drying Technology,* 22**,** 1983-2008.
ZHANG, J., DATTA, A. K. & MUKHERJEE, S. 2005. Transport processes and large deformation during baking of bread. *AIChE Journal,* 51**,** 2569-2580.
ZHANG, Z. & KONG, N. 2012. Nonequilibrium Thermal Dynamic Modeling of Porous Medium Vacuum Drying Process. *Mathematical Problems in Engineering,* 2012**,** 1-22.

LIST OF FIGURE:

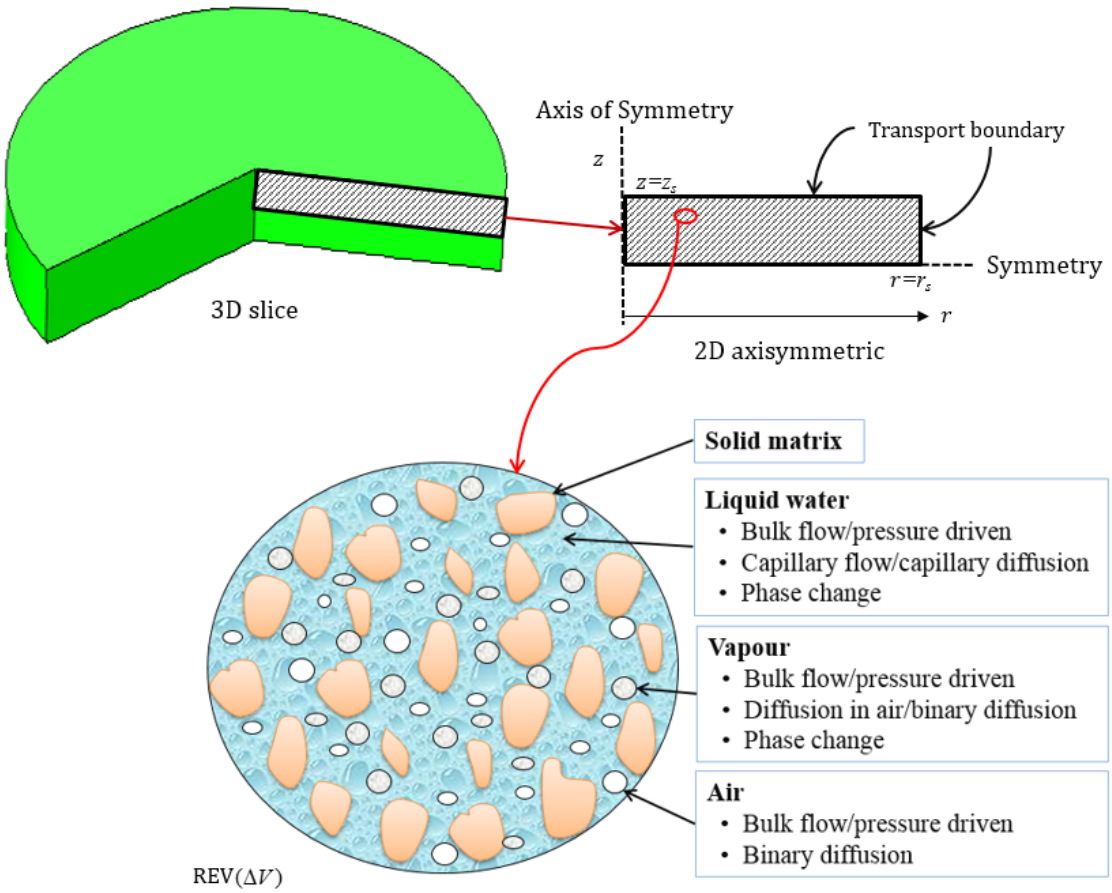

Fig. 1. Schematic showing 3D sample, 2D axisymmetric domain and representative elementary volume with the transport mechanism of different phases

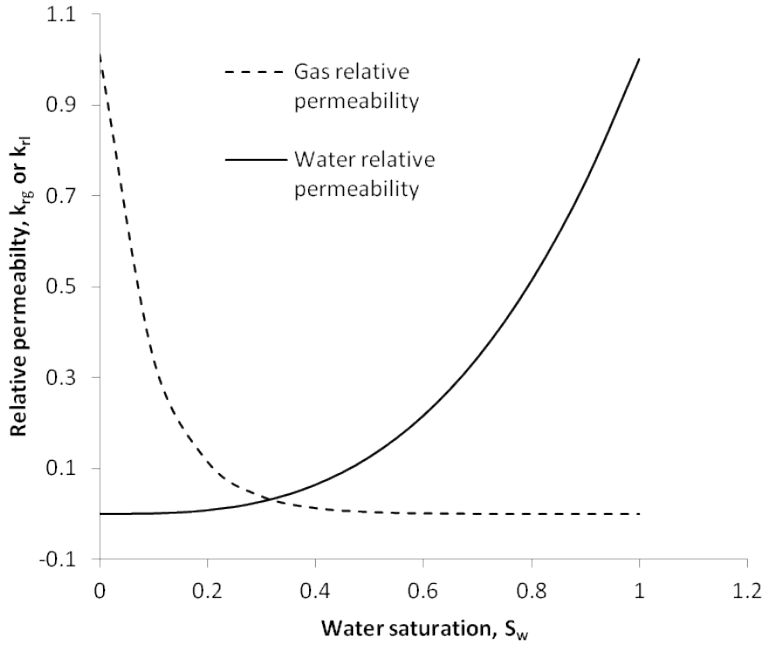

Fig. 2. Gas ($k_{r,g}$) and water ($k_{r,w}$) relative permeabilities of apple tissues as a function of saturation (Feng et al., 2004).

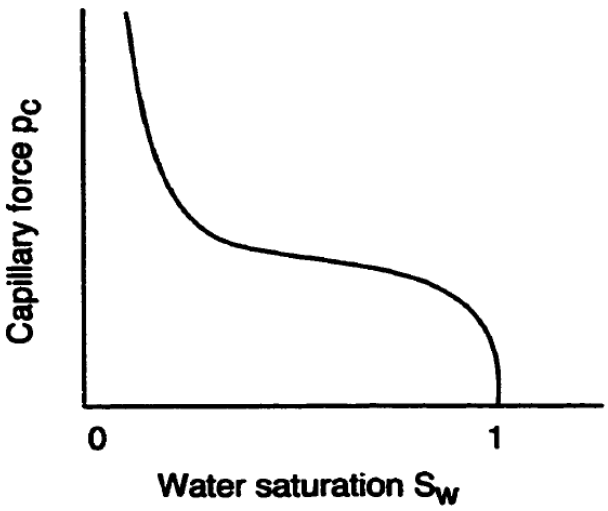

Fig. 3. Typical variation of capillary force as a function of liquid saturation in porous media (Bear, 1972)

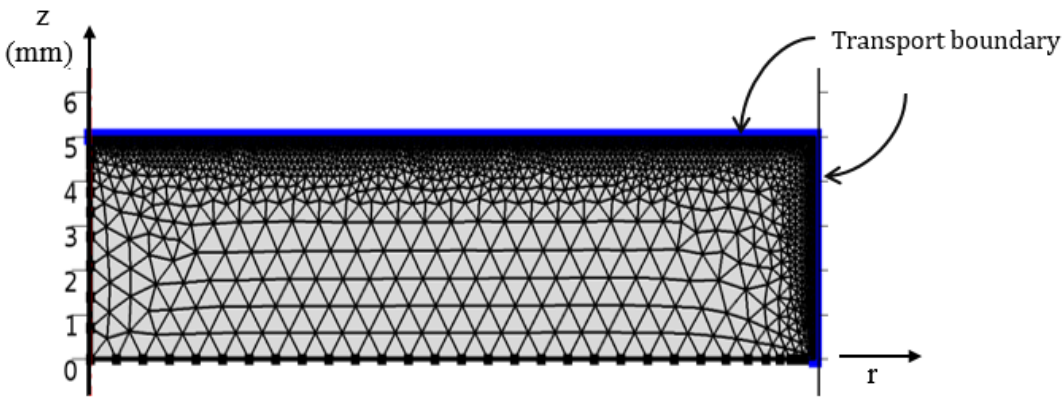

Fig. 4. Mesh for the simulation

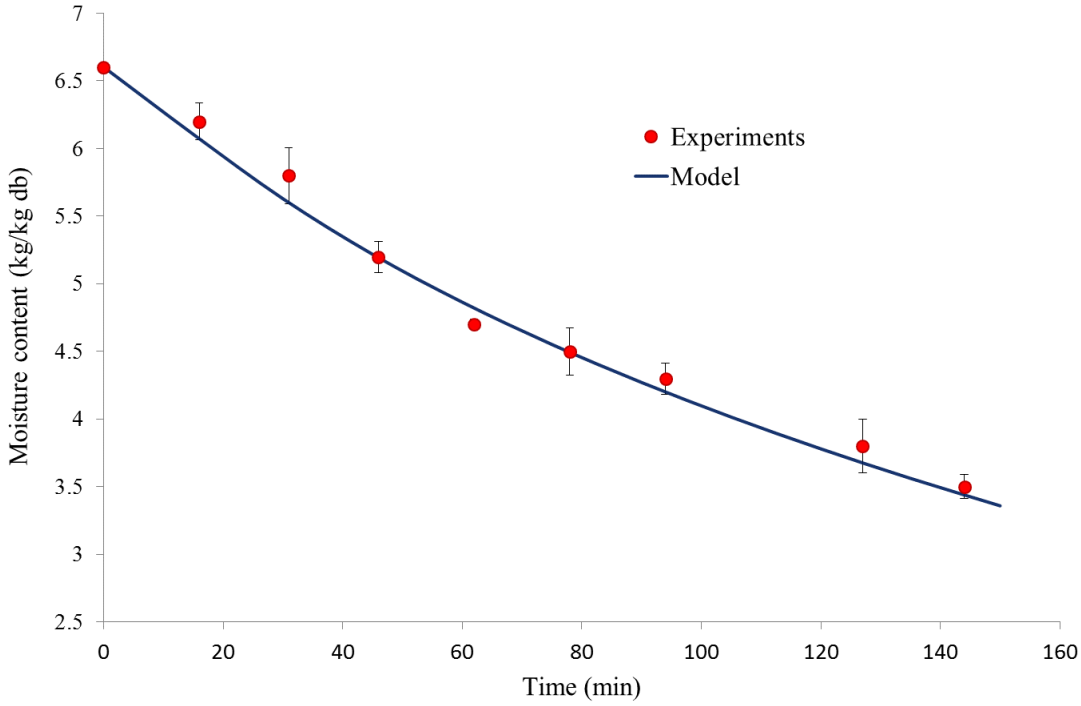

Fig. 5. Comparison between predicted and experimental values of average moisture content during drying

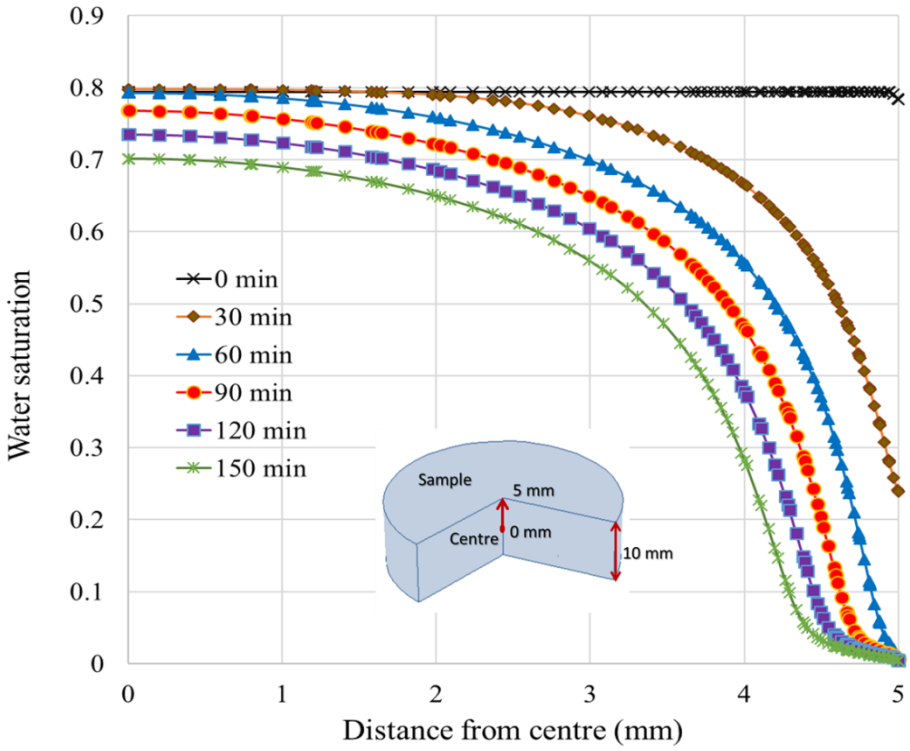

Fig. 6. Spatial distribution of water saturation with time

730

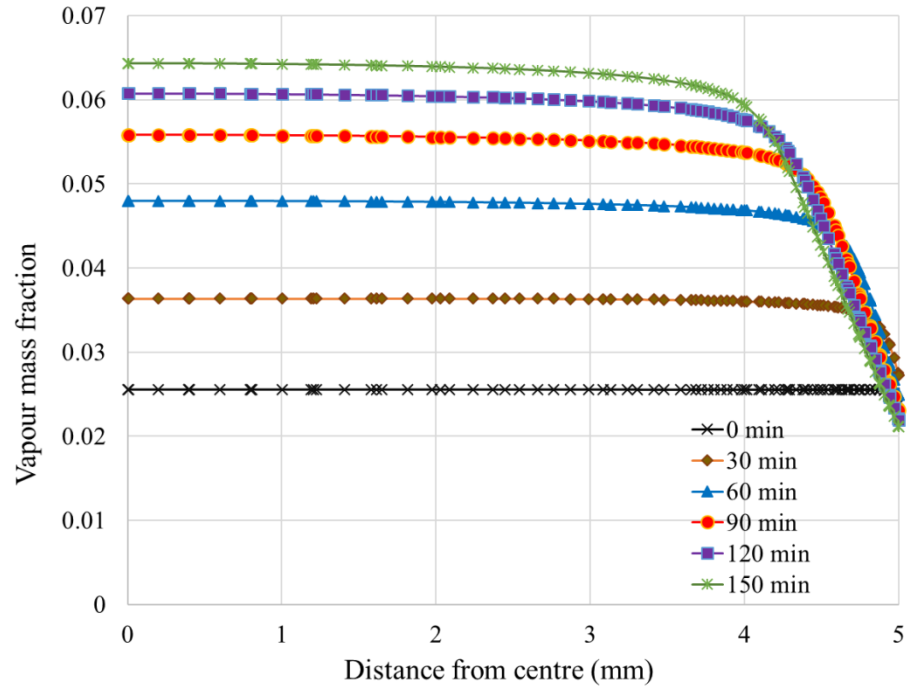

Fig. 7. Spatial distribution of vapour mass fraction with different time

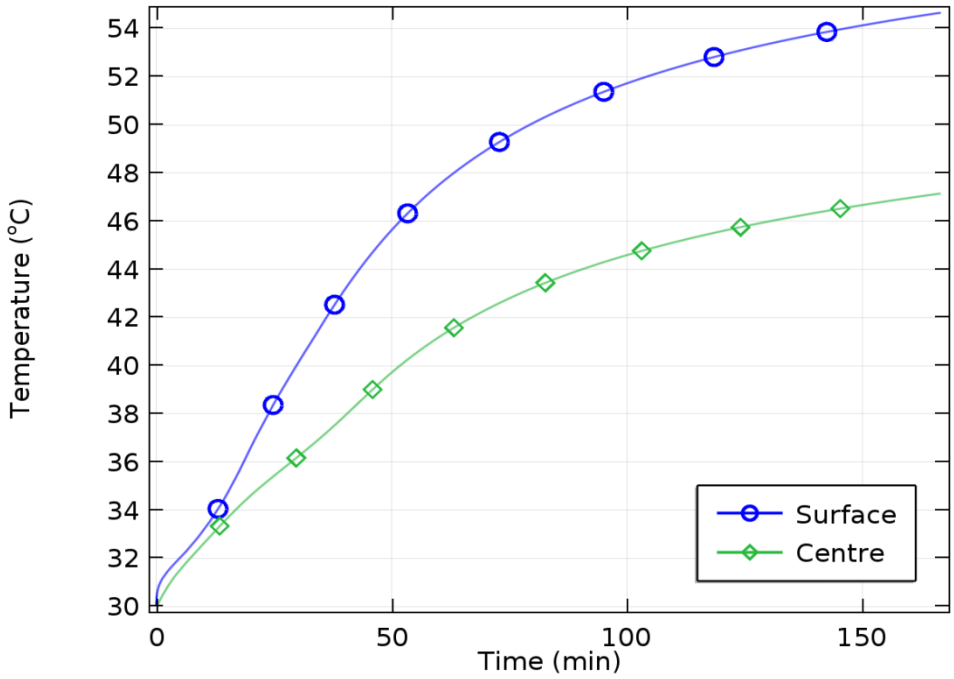

Fig. 8. Surface and centre temperature of the sample obtained from model

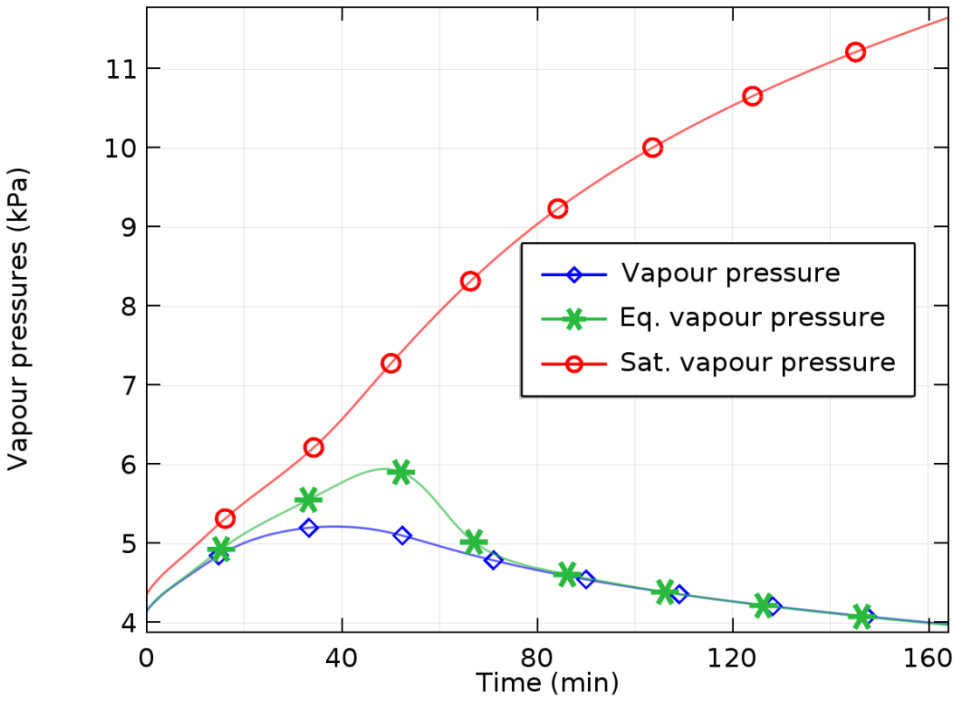

Fig. 9. Vapour pressure, equilibrium vapour pressure and saturation pressure 0.1 mm below the top surface of the sample

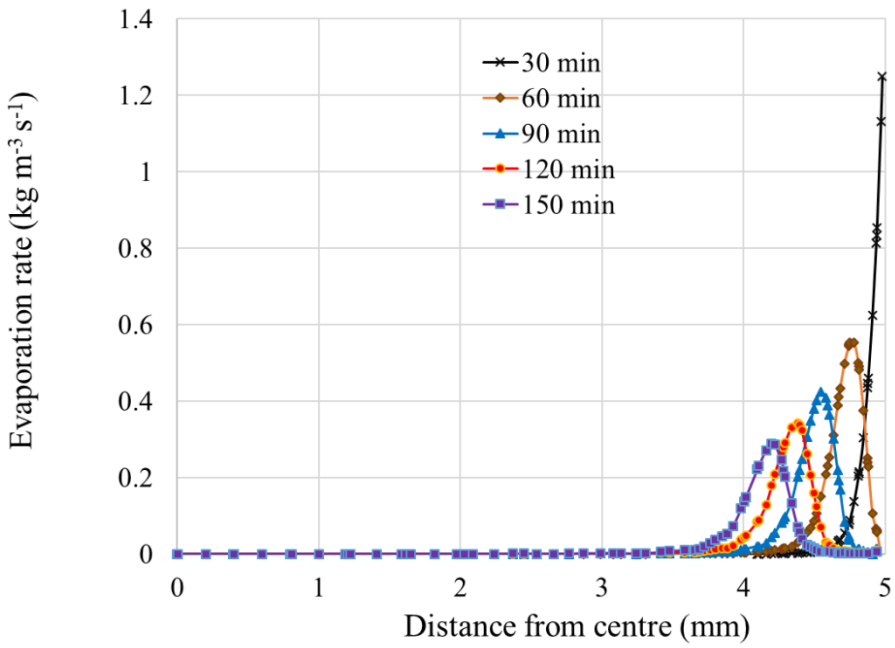

Fig. 10. Spatial distribution of evaporation rate at different drying times

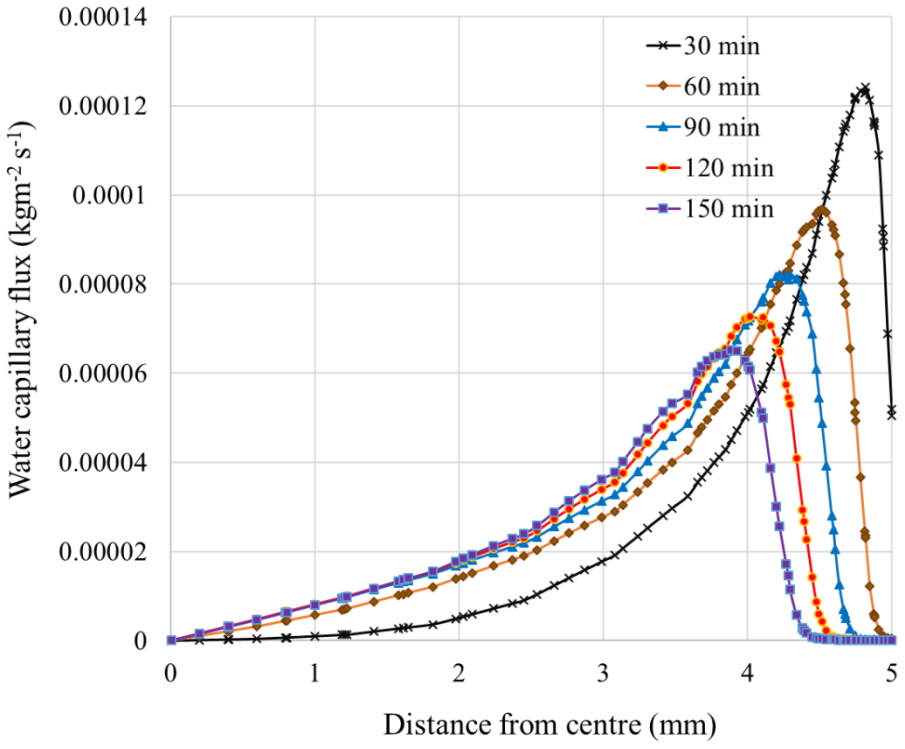

Fig. 11. Water flux due to capillary diffusion

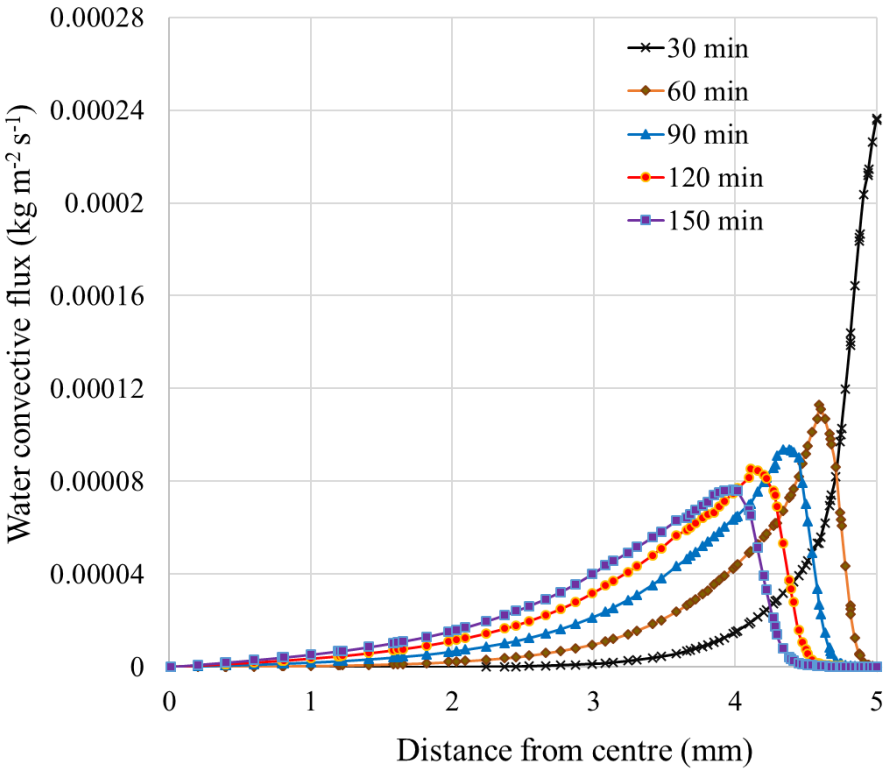

Fig. 12. Water flux due to gas pressure

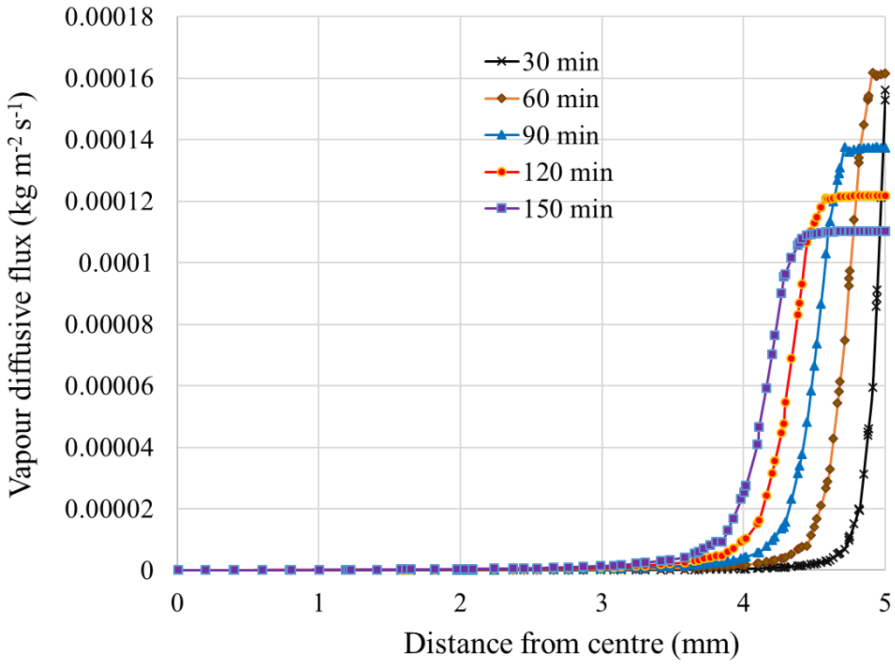

Fig. 13. Vapour flux due to binary diffusion

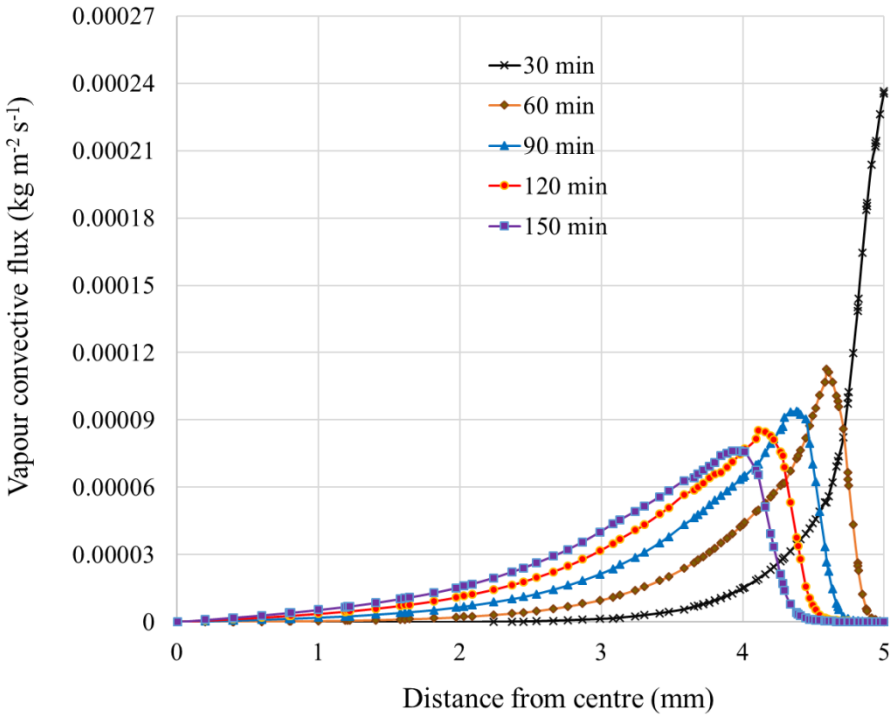

Fig. 14. Vapour flux due to gas pressure

LIST OF TABLES:

Table 1. Input properties for the model

Parameter	Value	Reference
Sample diameter, Dia_s	40 mm	This work
Sample thickness, Th_s	10 mm	This work
Equivalent porosity, initial, φ_0	0.922	(Rahman, 2008, Ni, 1997).
Water saturation, initial, S_{w0}	0.794	(Rahman, 2008, Ni, 1997).
Initial saturation of vapour, S_{v0}	0.15	(Rahman, 2008, Ni, 1997).
Gas saturation, initial,	0.19	(Rahman, 2008, Ni, 1997).
Initial temperature, T_0	303K	
Initial vapour mass fraction, w_{v0}	0.026	Calculated
Constants		
Evaporation constant, K_{evap}	1000	This work
Drying air temperature, T_{air}	333K	This work
Universal gas constant, R_g	8.314 J mol^{-1}K^{-1}	(Çengel and Boles, 2006)
Molar mass of water, M_w	18.016 g mol^{-1}	(Çengel and Boles, 2006)
Molar mass of vapour, M_v	18.016 g mol^{-1}	(Çengel and Boles, 2006)
Molar mass of gas (air), M_a	28.966 g mol^{-1}	(Çengel and Boles, 2006)
Latent heat of evaporation, h_{fg}	2.26e6 J kg^{-1}	(Çengel and Boles, 2006)
Ambient pressure, P_{amb}	$101325\ Pa$	
Thermo-physical properties		
Specific heats		
Apple solid, C_{ps}	3734 J kg^{-1}K^{-1}	Measured
Water, C_{pw}	4183 J kg^{-1}K^{-1}	(Carr et al., 2013a)
Vapour, C_{pv}	1900 J kg^{-1}K^{-1}	(Carr et al., 2013a)

Parameter	Value	Reference
Air, C_{pa}	1005.68 J kg^{-1}K^{-1}	(Carr et al., 2013a)
Thermal conductivity		
Apple solid, $k_{th,s}$	0.46 W m^{-1}K^{-1}	(Choi and Okos, 1986)
Gas, $k_{th,g}$	0.026 W m^{-1}K^{-1}	(Rakesh et al., 2012)
Water, $k_{th,w}$	0.644 W m^{-1}K^{-1}	(Rakesh et al., 2012)
Density		
Apple solid, ρ_s	1419 kg m^{-3}	This study
Vapour, ρ_v	Ideal gas law, kg m^{-3}	
Air, ρ_v	Ideal gas law, kg m^{-3}	